

Suzaku Observation of the Ophiuchus Galaxy Cluster: One of the Hottest Cool Core Clusters

Yutaka FUJITA,¹ Kiyoshi HAYASHIDA,¹ Masaaki NAGAI,¹ Susumu INOUE,^{2,3} Hironori MATSUMOTO,³
Nobuhiro OKABE,⁴ Thomas H. REIPRICH,⁵ Craig L. SARAZIN,⁶ and Motokazu TAKIZAWA⁷

¹*Department of Earth and Space Science, Graduate School of Science, Osaka University,
1-1 Machikaneyama, Toyonaka, Osaka 560-0043*

fujita@vega.ess.sci.osaka-u.ac.jp

²*National Astronomical Observatory of Japan, 2-21-1 Osawa, Mitaka, Tokyo 181-8588*

³*Department of Physics, Kyoto University, Kitashirakawa-Oiwake-cho, Sakyo-ku, Kyoto 606-8502*

⁴*Astronomical Institute, Graduate School of Science, Tohoku University, Sendai 980-8578*

⁵*Argelander Institute for Astronomy (AIfA), Bonn University, Auf dem Hügel 71, 53121 Bonn, Germany*

⁶*Department of Astronomy, University of Virginia, P.O. Box 400325, Charlottesville, VA 22904-4325, USA*

⁷*Department of Physics, Yamagata University, 1-4-12 Kojirakawa, Yamagata-city, Yamagata 990-8560*

(Received 2008 April 1; accepted 2008 June 23)

Abstract

We present the analysis of a Suzaku observation of the Ophiuchus galaxy cluster. We confirmed that the cluster has a cool core. While the temperature of the intracluster medium (ICM) decreases toward the center, the metal abundance increases. Except for the core ($r \lesssim 50$ kpc), the cluster is hot (~ 9 – 10 keV) and is almost isothermal for $r \lesssim 1$ Mpc; the latter contradicts a previous study. We do not detect any variation of the redshift of the ICM in the cluster; the upper limit of the velocity difference is 3000 km s^{-1} . The iron-line ratios in X-ray spectra indicate that the ICM has reached the ionization equilibrium state. From these results, we conclude that the Ophiuchus cluster is not a major merger cluster, but one of the hottest clusters with a cool core. We obtain the upper limit of non-thermal emission from the cluster, which is consistent with both the recent claimed detection with INTEGRAL and the recent upper limits with the Swift/BAT. If the cluster has bright non-thermal emission, as suggested by the INTEGRAL measurement, it is probably not due to a recent major cluster merger.

Key words: galaxies: clusters: general — galaxies: cooling flows — galaxies: intergalactic medium — X-rays: galaxies: clusters — X-rays: individual (Ophiuchus)

1. Introduction

The cold dark matter (CDM) model predicts that the typical mass of virialized objects in the Universe increases with time. This means that the most massive or hottest galaxy clusters ($kT \gtrsim 10$ keV) should be the objects that have formed most recently. In fact, X-ray observations have shown that the hottest clusters are often ‘major-merger’ clusters. These clusters are now growing through the mergers. For example, cluster 1E 0657–56 ($kT = 14.8^{+1.7}_{-1.2}$ keV) has a clear bow shock associated with a merger; a smaller cluster is penetrating a larger cluster with a velocity of 3000 – 4000 km s^{-1} (Markevitch et al. 2002). On the other hand, these hottest clusters are rarely ‘cool core clusters’, which have a distinct cool core and are almost isothermal outside the core. This is probably because cool cores are destroyed by cluster mergers (Ricker & Sarazin 2001; Fujita et al. 2002).

Cluster mergers may accelerate relativistic particles at shocks and in turbulent regions in the ICM (Jaffe 1977; Roland 1981; Schlickeiser et al. 1987; Sarazin 1999; Takizawa, Naito 2000; Fujita & Sarazin 2001; Brunetti et al. 2001; Miniati et al. 2001; Ohno et al. 2002; Fujita et al. 2003; Ryu et al. 2003; Brunetti & Blasi 2005; Cassano & Brunetti 2005; Inoue et al. 2005; Kang et al. 2007). With BeppoSAX, non-thermal hard X-ray emission from relativistic particles has

been detected from several clusters, such as the Coma cluster (Fusco-Femiano et al. 2004). Most of them are actually merging clusters (Nevalainen et al. 2004). However, the detections are still controversial (Rossetti & Molendi 2004), and confirmation with other instruments would be highly desirable. The Suzaku HXD has an improved sensitivity for hard X-rays (Takahashi et al. 2007), and attempts have been made to detect non-thermal hard X-ray emission from clusters. So far, no firm detections have been reported (Kawano et al. 2008).

The Ophiuchus cluster is one of the hottest known clusters. It has been observed with several satellites, such as HEAO 1 (Johnston et al. 1981), EXOSAT (Arnaud et al. 1987), Tenma (Okumura et al. 1988), and GINGA (Kafuku et al. 1992). Previous observations with ASCA and BeppoSAX showed that the temperature of the ICM is ~ 10 keV (Watanabe et al. 2001; Nevalainen et al. 2004). In addition to the high temperature, this cluster has a few interesting features. First, it has been reported to have a complicated temperature distribution, in particular, the temperature of its western part reaches ~ 20 keV (Watanabe et al. 2001). This temperature is comparable to that observed in 1E 0657–56 (Markevitch et al. 2002). Thus, this cluster may be undergoing a major merger that induces the motion of the ICM with a velocity of $\gtrsim 3000 \text{ km s}^{-1}$. Second, non-thermal hard X-ray emission may have been detected from the cluster. Nevalainen et al. (2004) searched for non-thermal

emission with BeppoSAX, and found some evidence at a 2σ level. Recently, Eckert et al. (2008) detected non-thermal emission from the center of the cluster with INTEGRAL at a 6.4σ level. However, a recent long exposure with the Swift/BAT instrument failed to detect any nonthermal emission, and set an upper limit below the claimed INTEGRAL detection (Ajello et al. 2008; Okajima et al. 2008).

In this paper, we report our observational results of the Ophiuchus cluster with Suzaku. Thanks to the low background of Suzaku (Mitsuda et al. 2007), we can obtain an X-ray spectrum even in regions far from the cluster center; we discuss the temperature and metal abundance distributions in the ICM. The high spectral resolution of the XIS (Koyama et al. 2007) on board Suzaku also enables us to measure or limit the bulk motion of the ICM. Moreover, the hard X-ray detector, HXD, can constrain the non-thermal emission from the cluster, which can be compared with the INTEGRAL and Swift/BAT results.

In this paper, we assume cosmological parameters of $\Omega_0 = 0.3$, $\lambda_0 = 0.7$, and $H_0 = 70 \text{ km s}^{-1} \text{ Mpc}^{-1}$. Since the cluster redshift is $z = 0.028$ (Lahav et al. 1989), one arc-minute corresponds to 33 kpc. All statistical errors are given at the 90% confidence level, unless otherwise mentioned.

2. Observations

We observed the Ophiuchus cluster with Suzaku on 2007 March 21–24 for a total exposure time of 105 ks. Figure 1 shows a mosaic image of the cluster obtained with the XIS; the field of view (FOV) of the XIS is $17'.8 \times 17'.8$. We observed five regions with the XIS: C (central), N (north), W (west), S (south), and E (east) regions. The exposure time for region C is 15 ks, and those for other regions are 22.5 ks. The XIS

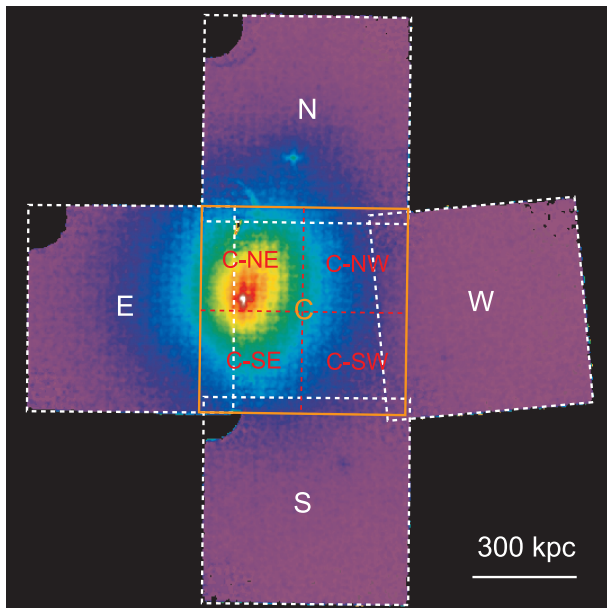


Fig. 1. Mosaic image of the Ophiuchus cluster obtained with Suzaku XIS. For each of the five pointings, the images from the three XIS detectors (XIS 0, XIS 1, and XIS 3) were combined. The image is corrected for vignetting, but not for background. The calibration sources at the corners of the fields were excluded. Regions used for spectral analysis are shown.

was operated in the normal full-frame clocking mode. The edit mode was 3×3 and 5×5 and we combined the data of both modes for our analysis. We employed the following calibration files: HXD (20071201), XIS (20071122), and XRT (20070622). Events with ASCA grades of 0, 2, 3, 4, and 6 were retained. We excluded the data obtained at the South Atlantic Anomaly, during Earth occultation, and at the low elevation angles from Earth rim of $< 5^\circ$. For the XIS data, we further excluded the data with elevation angle from the rim of the shining Earth smaller than 20° . For the HXD data, we removed the data obtained at the locations where the Cut-Off-Rigidity (COR) is lower than 6 GV.

3. Spectral Analysis

Our spectral analysis is similar to that in Fujita et al. (2008). We extract X-ray spectra for the five regions (C, W, S, E, and N) shown in figure 1. For the central region (C), we also analyze the square subsections (C-NW, C-SW, C-SE, and C-NE). We calculated the effective area for each XIS chip using XISSIMARFGEN, which provides the ancillary response file (ARF) through Monte Carlo simulations (Ishisaki et al. 2007). All spectra were rebinned to give a minimum of 50 raw counts per spectral bin to allow χ^2 statistics to be applied. The non-X-ray instrumental background (NXB) spectrum is subtracted from the spectrum of each region. The NXBs for individual regions were constructed from night Earth data, and were generated by the routine XISNXBGEN included in Suzaku FTOOLS Ver. 7, including the time-variation of the NXB (Tawa et al. 2008). We always include the NXB in all of the following spectral fits.

Using XSPEC (Ver. 12), the spectra of the three XISs are simultaneously fitted with a single thermal model (APEC) representing the ICM and with the Galactic absorption (WABS: N_{H}). The parameters of these models are set to be the same for all the XISs, except for the normalization of the APEC model, which is the main component of the spectra. While the normalizations for the two front-illuminated (FI) chips (XIS 0 and 3) are the same, that for the Back-Illuminated (BI) chip (XIS 1) is allowed to have an independent value, because of the residual calibration inaccuracies between FI and BI. In the fits, we also consider the contributions of the cosmic X-ray background (CXB) and the Galactic soft X-ray emission. The CXB spectrum is given by a power-law with an index of 1.412 and the flux in the 2–10 keV band is $F_{\text{CXB}} = 6.38 \times 10^{-8} \text{ erg cm}^{-2} \text{ s}^{-1} \text{ sr}^{-1}$ (Kushino et al. 2002). We call this CXB spectrum ‘the normal CXB spectrum’. The Galactic soft X-ray emission model is constructed on the model of Snowden et al. (1998).¹ The emission consists of two thermal components with temperatures of $kT \approx 0.1 \text{ keV}$ (the local hot bubble) and 0.3 keV (the Milky Way halo); the values are slightly dependent on the region observed. The metal abundance and the redshift of both components are solar and zero, respectively. The parameters for the Galactic soft X-ray emission are fixed in the fits, except for the overall normalization; the relative normalization between the two components is fixed at cooler/warmer ≈ 0.15 , which is provided by the Galactic soft

¹ (<http://heasarc.gsfc.nasa.gov/cgi-bin/Tools/xraybg/xraybg.pl>).

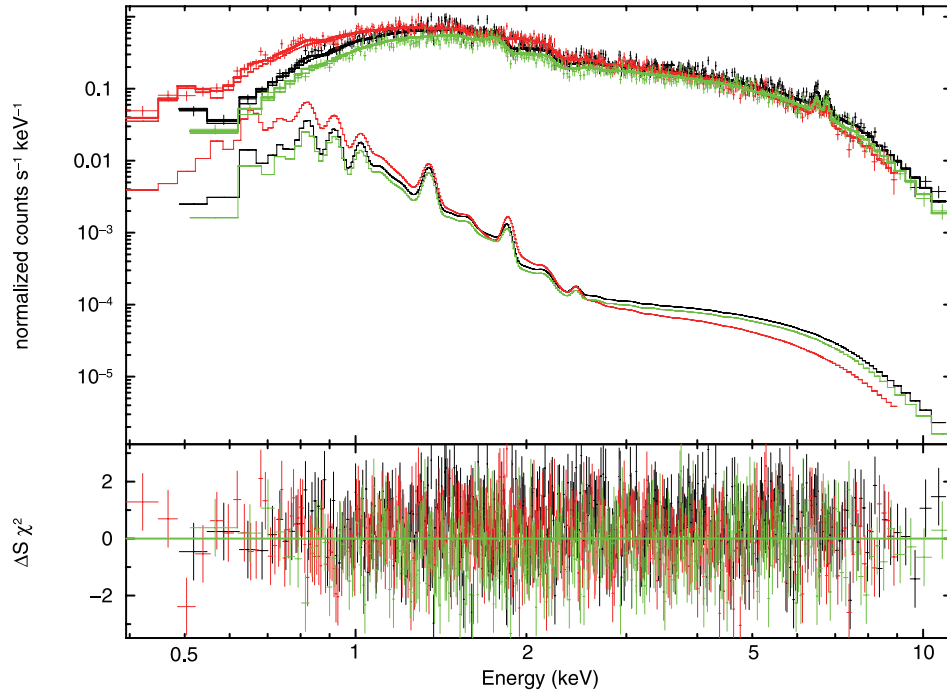


Fig. 2. XIS spectra for region C-NW (crosses). The results of the fit are shown by the solid lines; the lower lines are the background emission (CXB plus the Galactic one). The lower panel plots the residuals divided by the 1σ errors. The NXB spectra have been subtracted.

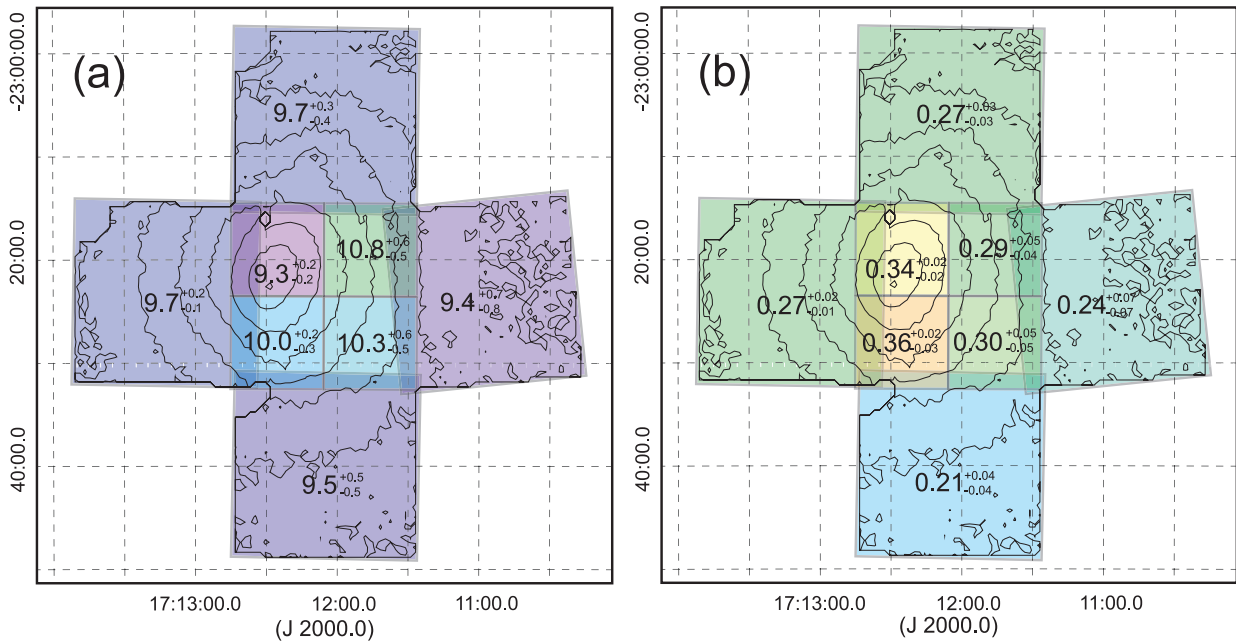


Fig. 3. (a) Temperature map of the Ophiuchus cluster. The numbers represent the temperatures (keV) for each region. X-ray brightness contours (logarithmically spaced by a factor of 2) are overlaid. (b) Same as (a), but for metal abundance (Z_{\odot}).

X-ray emission model.¹ While the ARFs for the ICM emission were constructed by assuming that it follows a beta model for the cluster ($\beta = 0.747$ and the core radius of $6'$: Reiprich & Böhringer 2002), those for the background emission (CXB plus the Galactic one) were made by assuming that the emission is spatially uniform. Figure 2 shows the spectra of the

three XISs for a region with typical photon counts for the spectral analysis (C-NW) and the result of the fit.

Table 1 shows the results of the spectral fits. Temperatures (T) and abundances (Z) are also shown in figure 3. In determining T , Z , and the absorbing column N_{H} , the redshift of the ICM is fixed at the optical value of $z = 0.028$

Table 1. The results of spectral fits and redshifts.

Region	kT (keV)	Z (Z_{\odot})	N_{H} (10^{21} cm^{-2})	χ^2/dof	z
C	$9.7^{+0.1}_{-0.2}$	$0.33^{+0.02}_{-0.01}$	$3.1^{+0.1}_{-0.0}$	5399.08/5044
C-NW	$10.8^{+0.6}_{-0.5}$	$0.29^{+0.05}_{-0.04}$	$2.5^{+0.2}_{-0.1}$	1326.70/1176	0.0319 ± 0.0020
C-SW	$10.3^{+0.6}_{-0.5}$	$0.30^{+0.05}_{-0.05}$	$2.8^{+0.2}_{-0.3}$	1042.62/ 936	0.0292 ± 0.0028
C-SE	$10.0^{+0.2}_{-0.3}$	$0.36^{+0.02}_{-0.03}$	$3.2^{+0.1}_{-0.1}$	2935.76/2602	0.0290 ± 0.0013
C-NE	$9.3^{+0.2}_{-0.2}$	$0.34^{+0.02}_{-0.02}$	$3.3^{+0.1}_{-0.0}$	3768.32/3732	0.0297 ± 0.0011
N	$9.7^{+0.3}_{-0.4}$	$0.27^{+0.03}_{-0.03}$	$2.4^{+0.1}_{-0.1}$	2425.38/2221	0.0309 ± 0.0017
W	$9.4^{+0.7}_{-0.8}$	$0.24^{+0.07}_{-0.07}$	$1.4^{+0.2}_{-0.2}$	909.52/ 877	0.0287 ± 0.0054
S	$9.5^{+0.5}_{-0.5}$	$0.21^{+0.04}_{-0.04}$	$1.8^{+0.2}_{-0.1}$	1499.63/1375	0.0283 ± 0.0025
E	$9.7^{+0.2}_{-0.1}$	$0.27^{+0.02}_{-0.01}$	$2.9^{+0.1}_{-0.0}$	4187.73/4028	0.0305 ± 0.0011
ASCA	$10.0^{+0.3}_{-0.3}$	$0.34^{+0.04}_{-0.04}$	3.0 (Fixed)	66.6 / 45
BeppoSAX	$9.1^{+0.6}_{-0.5}$	$0.49^{+0.08}_{-0.08}$
Suzaku HXD	$9.0^{+0.3}_{-0.3}$	0.3 (Fixed)	0.0 (Fixed)	133.92/ 152

(Lahav et al. 1989). The spectral fits show that the cluster is almost isothermal with a temperature of $kT \sim 9\text{--}10$ keV and an abundance of $Z \sim 0.3 Z_{\odot}$. When we derive the errors, we vary the normalization of the CXB in order to include possible field-to-field variance. Kushino et al. (2002) derived a 1σ deviation of the CXB intensity to be $6.49^{+0.56}_{-0.61}\%$ using ASCA GIS data. We roughly estimate that the CXB uncertainty for the XIS field is $6.49\sqrt{0.4/0.088} \sim 14\%$, considering the typical size of the area studied in Kushino et al. (2002) ($\sim 0.4 \text{ deg}^2$) and the FOV of the XIS ($\sim 0.088 \text{ deg}^2$). Note that this value depends on the flux threshold to resolve point sources. While Kushino et al. (2002) employed $2 \times 10^{-13} \text{ erg s}^{-1} \text{ cm}^{-2}$ (2–10 keV), we have excluded point sources with smaller fluxes. Thus, the actual uncertainty might be smaller. We fit the XIS spectra of regions C, N, W, S, and E for 14% higher or lower CXB normalizations than that of the normal CXB spectrum, and derive temperatures and metallicities. By adding linearly the statistical errors of the fits to this CXB uncertainty, we obtain the errors. Similarly, we assume $\sim 28\%$ uncertainty for the CXB normalizations for the four smaller regions in C. In table 1, N_{H} shows a large variation. Given that such large variations and values are not seen in clusters at higher Galactic latitudes, this variation is likely to be Galactic.

For comparison, we also present the results of previous studies in table 1. The ASCA data are for the central region of the cluster (region 2 in Watanabe et al. 2001). They are consistent with the Suzaku results for region C. The HXD results will be discussed in section 6.

4. Deprojection Analysis

The Chandra image of the Ophiuchus cluster exhibits cold fronts around the core (Ascasibar & Markevitch 2006). Numerical simulations have shown that the region surrounded by cold fronts has a low temperature compared with the outside of the cold fronts (Fujita et al. 2004a; Ascasibar & Markevitch 2006), which is consistent with observations for several clusters (e.g., Markevitch et al. 2001; Mazzotta & Giacintucci

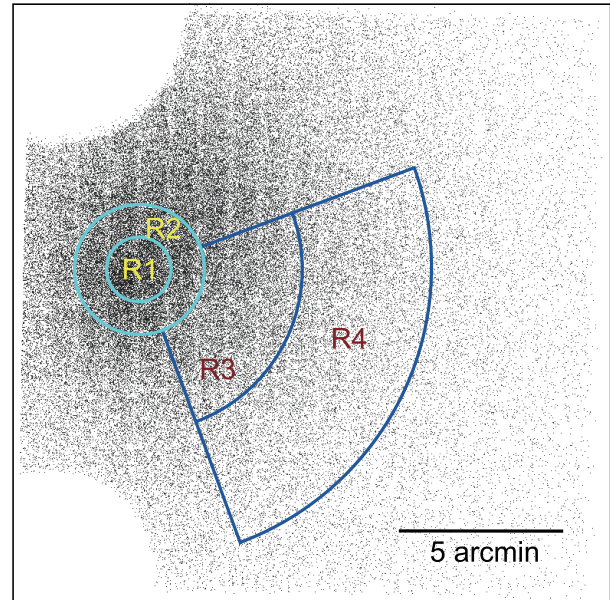


Fig. 4. XIS 0 sky image of region C. The regions used for a deprojection analysis are shown.

2008). In order to study the temperature and metal abundance of the core in detail, we made a deprojection analysis to remove projection effects. The deprojection procedure we adopted is the same as that in Blanton, Sarazin, and McNamara (2003) and Fujita et al. (2004b).

We choose annuli and sectors centered on the X-ray peak, as shown in figure 4. We fix the Galactic absorption at the value of region C ($N_{\text{H}} = 3.1 \times 10^{21} \text{ cm}^{-2}$; table 1). The Galactic soft X-ray emission is also fixed at the values of region C. The CXB is fixed at the normal value. These background models are always included in the following procedure.

First, we fit the spectrum from region R4 with a single ICM model (APEC). Then, the next annulus (R3) is fitted. The model used for this annulus is a combination of the best-fitting

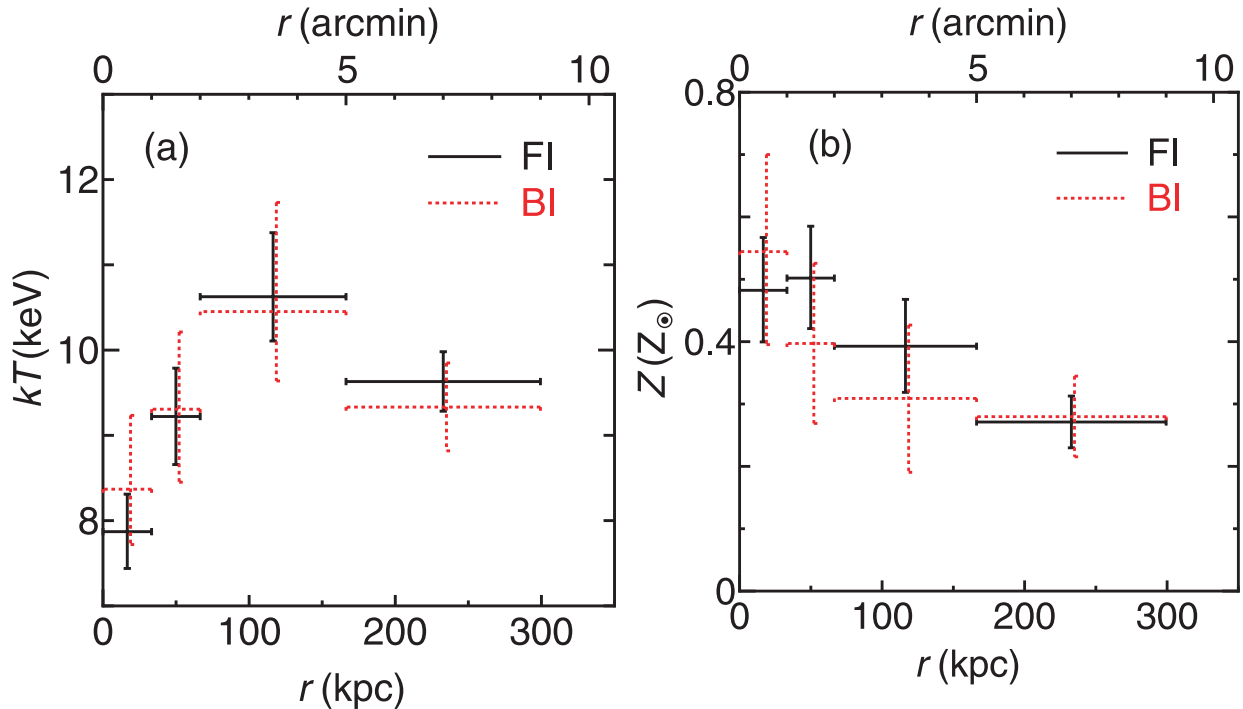


Fig. 5. (a) Temperature and (b) metal abundance profiles as functions of the distance from the cluster center.

model of the exterior annulus with the normalization scaled to account for the spherical projection of the exterior shell onto the inner one, along with another APEC component added to account for the emission at the radius of interest. This process is continued inward, and we fitted one spectrum at a time. The FI and BI chip are treated separately because of their different spectral responses.

The results of the fits are shown in figure 5. The temperature of the ICM decreases to $kT \sim 8$ keV toward the cluster center, while the abundance increases to $Z \sim 0.5\text{--}0.6 Z_{\odot}$. This behavior is often found in cool core clusters (Fukazawa et al. 1994; Finoguenov et al. 2001; De Grandi & Molendi 2001; Pointecouteau et al. 2005; Vikhlinin et al. 2005; Piffaretti et al. 2005). These results are conservative because, considering point-spread-function (PSF) smearing by the angular resolution of Suzaku ($\sim 2'$ half power diameter, independent of energy), the actual central temperature and abundance will be even lower and higher, respectively.

5. Bulk Motion of the ICM

By measuring the redshifts of metal lines in X-ray spectra, we can estimate the velocity of the ICM. There have been a number of previous attempts to measure bulk motions in the ICM using X-ray line shifts (e.g., Dupke & Bregman 2006). Since the XISs on board Suzaku have an excellent spectral resolution, they are suitable for such studies (Ota et al. 2007). In this section, we estimate the bulk motion of the ICM of the Ophiuchus cluster.

We investigate the redshifts of the ICM for four central regions (C-NW, C-SW, C-SE, and C-NE) and the four surrounding regions (N, W, S, and E) shown in figure 1. A ‘gain

correction’ of the CCD chips in instruments like the XIS must be done carefully for a precision measurement of the redshift of the metal lines. The XISs are always illuminated by calibration sources (^{55}Fe) that appear as a Mn $K\alpha$ line (5.895 keV) in spectra if not masked. In this section, we treat the three XIS chips separately in order to allow for the gain difference among them. First, we limited the energy range to 5–8 keV and fit the ICM spectra including the emission from the calibration sources with bremsstrahlung and Gaussian line components. The Mn $K\alpha$ line from the calibration sources and the Fe K lines from the ICM are each fitted with the Gaussian components. We put the Gaussian components for the Fe K lines just because they may influence the line center of Mn $K\alpha$ line; we do not use them for determining the redshift. The central energy of the Mn $K\alpha$ line determined by this fit is referred to as $E_{\text{obs}}(\text{Mn } K\alpha)$. The gain correction factor is given by

$$f_{\text{gain}} = \frac{E_{\text{obs}}(\text{Mn } K\alpha)}{E_0(\text{Mn } K\alpha)}, \quad (1)$$

where $E_0(\text{Mn } K\alpha)$ is the true energy (5.895 keV). Typically, $|f_{\text{gain}} - 1| \lesssim 0.001$, and the uncertainty of f_{gain} is ~ 0.001 . On the other hand, we determine the redshift of the ICM, z_{fit} , through a spectral fit that is the same as that in section 3, but for each chip. Thus, a gain-corrected redshift is given by

$$z_{\text{gain}} = f_{\text{gain}}(z_{\text{fit}} + 1) - 1. \quad (2)$$

We present z_{gain} for each region in figure 6. The values averaged for the three XISs are shown in table 1. For regions W and S, only data for FI chips (XIS 0, and 3) are shown, because the BI chip (XIS 1) is less sensitive to hot gas ($\gtrsim 2$ keV), and the redshifts cannot be constrained. The redshifts in figure 6 are consistent with being constant, and the average

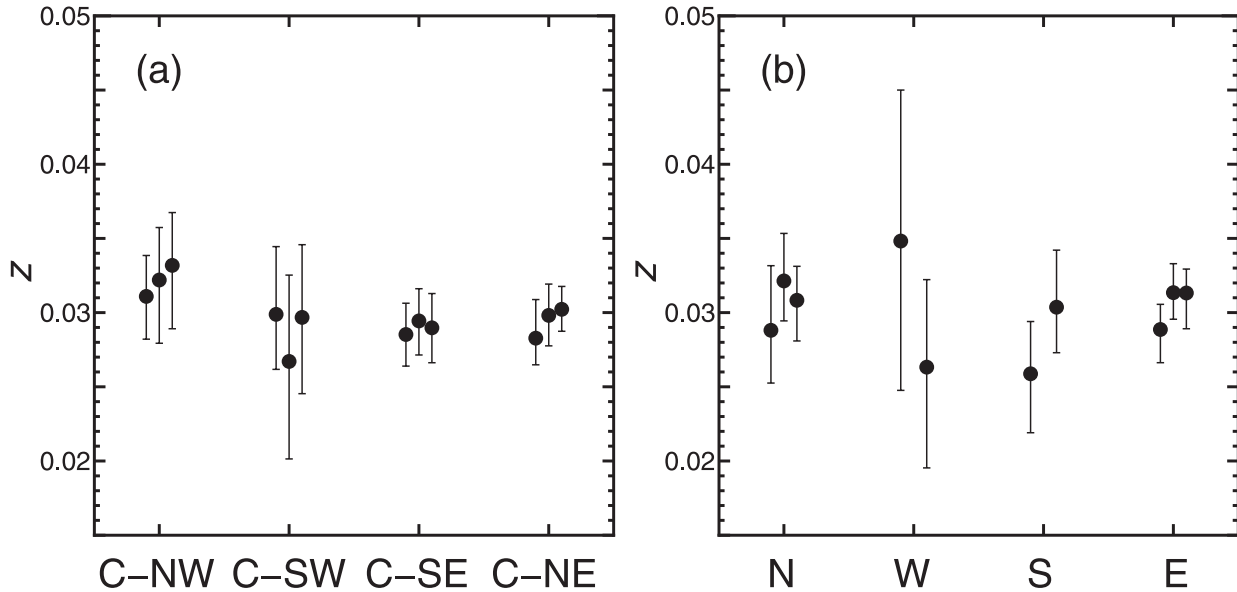


Fig. 6. Redshifts of the ICM in the (a) central regions and (b) surrounding regions. The three filled circles for each region are the gain-corrected redshifts (z_{gain}) for XIS 0, 1, and 3 from left to right. For regions W and S, only data from the FI chips (XIS 0, and 3) are shown.

is $z = 0.030 \pm 0.003$, which agrees with the optical redshift of the cluster ($z = 0.028$). The difference of the maximum (C-NW) and minimum redshift (W) in table 1 is $\lesssim 0.01$, which means that the velocity difference between different regions is $\lesssim 3000 \text{ km s}^{-1}$.

6. Non-Thermal Hard X-Ray Emission

The Suzaku HXD PIN detector is sensitive to hard X-rays ($\gtrsim 10 \text{ keV}$), and has a wider FOV ($34' \times 34'$ full width at half maximum, FWHM) than that of the XIS ($17'.8 \times 17'.8$). Although the center of the HXD field is shifted from that of the XIS field by $\sim 3'.5$, the shift is much smaller than the size of the HXD field. Thus, all of the five HXD fields (corresponding to the XIS fields C, N, W, S, and E) cover at least partially the central region of the cluster, where INTEGRAL detected hard X-ray excess emission (Eckert et al. 2008).

After correcting for dead time, the exposure times of the five fields are 12.6, 18.1, 19.4, 20.0, 20.1 ks for C, N, W, S, and E, respectively. We fit the HXD spectra with a thermal model (APEC), which represents the ICM, as well as a CXB component. We first simultaneously fit the spectra of the five fields. A redistribution matrix file for the HXD nominal position is used for the ICM emission. The ARFs of the ICM emission for each spectrum are generated with HXDARFGEN and ADDARF by assuming that the emission follows the same beta model that we adopted for the XIS (section 3). We fix the metal abundance of the APEC model at $0.3 Z_{\odot}$ and the redshift at $z = 0.028$ (optical redshift). The CXB is assumed to be uniform in a $2^{\circ} \times 2^{\circ}$ field, and a corresponding redistribution matrix file is employed. The spectrum of the CXB is represented by a power-law model multiplied by a HIGHECUT model in XSPEC. We adopt the power-law index of 1.29, the power-law normalization of $9.412 \times 10^{-9} \text{ photons cm}^{-2} \text{ s}^{-1} \text{ FOV}^{-1} \text{ keV}^{-1}$, the cutoff energy of $1 \times 10^{-4} \text{ keV}$, and the e-folding energy of

40 keV, following a standard model.² Thus, the free parameters for the fit are the temperature and normalization of the APEC model. While the temperature is common, the normalization is allowed to vary among the five spectra. We do not consider the Galactic absorption because it does not affect the results in the HXD energy band. The NXB spectra created from the pinxb_ver2.0_tuned NXB model are employed as a normal NXB. We find that the five spectra can be fitted with the thermal model with a temperature of $kT = 8.9^{+0.2}_{-0.4} \text{ keV}$. The normalizations of the five spectra agree with each other within $\pm 10\%$.

We thus combine the five spectra into one, and perform a fit again. The NXB spectra and the ARF are combined, correspondingly. The result of the fit is $kT = 9.0^{+0.3}_{-0.3} \text{ keV}$ (table 1 and figure 7). The spectrum does not require an extra hard X-ray component. The flux of the thermal component in 20–80 keV band is $6.8 \times 10^{-11} \text{ erg s}^{-1} \text{ cm}^{-2}$, which is about 20% higher than that expected from the BeppoSAX PDS observations (Nevalainen et al. 2004).

We note that the systematic uncertainty in the HXD NXB strongly affects the results. According to T. Mizuno (2007)³ the systematic 1σ uncertainty in the 15–40 keV NXB is 3.2%. We conservatively adopt a systematic uncertainty of $\pm 5\%$ (90% uncertainty), and estimate the upper limit on any extra hard X-ray component. Since the uncertainty in the NXB overwhelms the statistical error on the ICM temperature, we fix the temperature of the APEC model at 9.0 keV, and add a power-law component to represent the extra hard X-ray emission. We fixed the photon index of the power-law at 2.0, which is the same as that in Eckert et al. (2008). The 90% upper limit on the hard power-law component is obtained by employing the NXB spectra, for which normalization is 5% lower than the normal NXB. The HXD spectra

² (http://heasarc.nasa.gov/docs/suzaku/analysis/pin_cxb.html).

³ (<http://www.astro.isas.jaxa.jp/suzaku/doc/suzakumemo/suzakumemo-2007-09.pdf>).

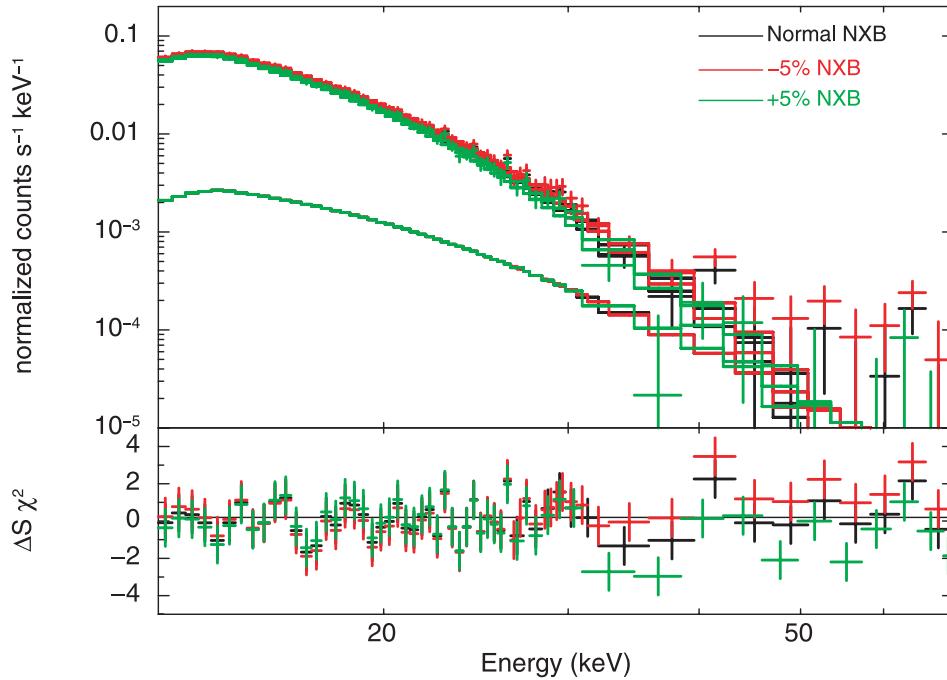


Fig. 7. HXD PIN spectra, including the effect of varying the normalization of the NXB by $\pm 5\%$ (crosses). The NXB has been subtracted. The fit (solid line) is for the normal NXB. The lower panel plots the residuals divided by the 1σ errors.

including $\pm 5\%$ variations in the normalization of the NXB are shown in figure 7. The upper limit on the flux of any extra hard X-ray component is $2.8 \times 10^{-11} \text{ erg s}^{-1} \text{ cm}^{-2}$ (20–60 keV), which is consistent with the detection obtained with INTEGRAL ($0.7\text{--}1.3 \times 10^{-11} \text{ erg s}^{-1} \text{ cm}^{-2}$; Eckert et al. 2008), and the upper limit from a combined Swift/BAT and Chandra spectrum ($4.5 \times 10^{-12} \text{ erg s}^{-1} \text{ cm}^{-2}$; Ajello et al. 2008). If we assume that the temperature of the APEC model is 8.5 keV, as Eckert et al. (2008) did, the upper limit on the flux is $4.1 \times 10^{-11} \text{ erg s}^{-1} \text{ cm}^{-2}$ (20–60 keV). On the other hand, if we assume that the ICM temperature is 9.7 keV (region C; table 1), it is $1.0 \times 10^{-11} \text{ erg s}^{-1} \text{ cm}^{-2}$. Note that the higher temperature is closer to the value found by Ajello et al. (2008).

7. Ionization Equilibrium

The high spectral resolution of Suzaku makes it possible to discuss the ionization equilibrium state of the ICM by measuring the intensity ratio of the hydrogen-like Fe $K\alpha$ line to the helium-like Fe $K\alpha$ line. We limited the energy range to 5–8 keV. The spectral components other than the ICM are the same as those in section 3. We fit the ICM component with a Bremsstrahlung model and two Gaussians. The spectra of the three XISs are fitted simultaneously.

Figure 8 shows the XIS spectra around the iron lines in region C-SE. Figure 9 shows the relation between the line ratios and the temperatures listed in table 1. The data include those for the three central regions (C-NW, C-SW, C-SE) and regions N, S, and E; the ratio for region W cannot be constrained, and that for region C-NE is omitted because this region is multi-temperature (figure 5a). For comparison, we present the relation predicted by the APEC model and those predicted by the NEI model (Ver. 2), which is based on the

Astrophysical Plasma Emission Database (APED; Smith et al. 2001). While APEC is a model for plasmas in ionization equilibrium, NEI is a model for those not in equilibrium. In figure 9, the observational data are generally consistent with the APEC model. The NEI model indicates $n_{et} \gtrsim 3 \times 10^{12} \text{ s cm}^{-3}$, where n_{et} is the ionization parameter. The results of NEI as well as APEC indicate that the ICM has reached ionization equilibrium. They may also indicate that the ICM, except for the core, consists of a single-temperature plasma and the cluster has no region strongly locally heated by a merger (see Ota et al. 2008). Although $n_{et} = 1 \times 10^{13} \text{ s cm}^{-3}$ is almost equivalent to ionization equilibrium for NEI, there is a small difference between NEI and APEC (figure 9). This may be due to the difference in the atomic physics of each model assumed.

8. Discussion

8.1. Comparison with ASCA Results

Although the Suzaku results are consistent with the previous ASCA results for the central region of the cluster (table 1), they are not for the outer regions. The results of ASCA indicated that the Ophiuchus cluster has a large temperature variation (Watanabe et al. 2001). In particular, the temperatures of the western and southern regions were reported to be extremely high ($kT \sim 15\text{--}20 \text{ keV}$). On the other hand, our Suzaku results indicate that the cluster is almost isothermal ($kT \sim 9\text{--}10 \text{ keV}$).

One possible cause for the difference would be a problem with the X-ray background for the ASCA observation. While Watanabe et al. (2001) used a background obtained from a source-free region near the cluster (H 1705–250), we constructed a background based on a model of the Galactic emission¹ plus a model for the hard CXB. Since the western and southern regions are dim, the difference of the background

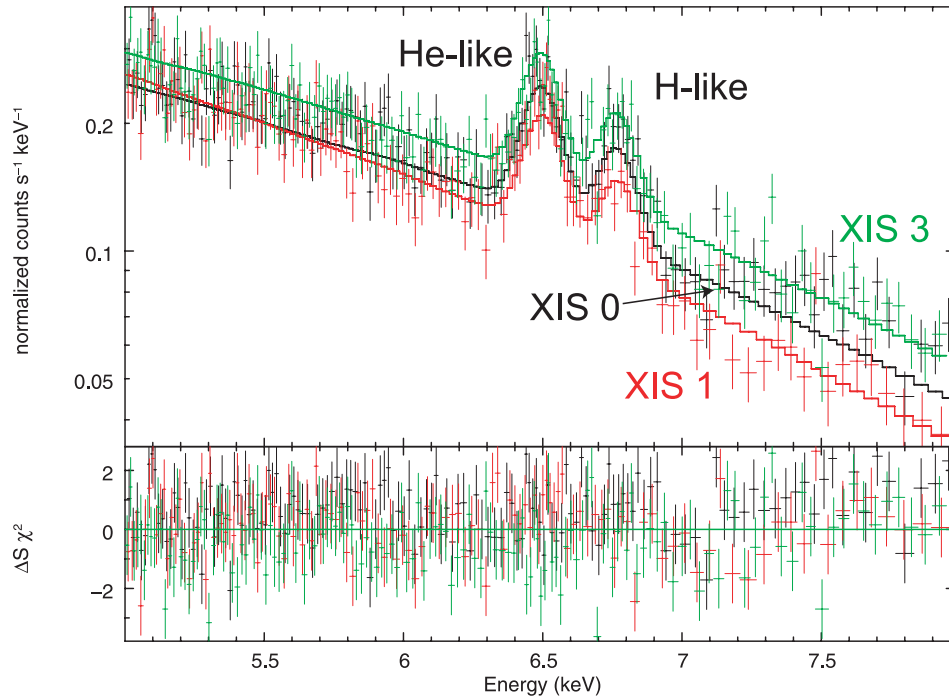


Fig. 8. XIS spectra around the Fe $K\alpha$ lines (crosses) and the results of the fit (solid lines) for region C-SE. The NXB spectra have been subtracted. The lower panel plots the residuals divided by the 1σ errors.

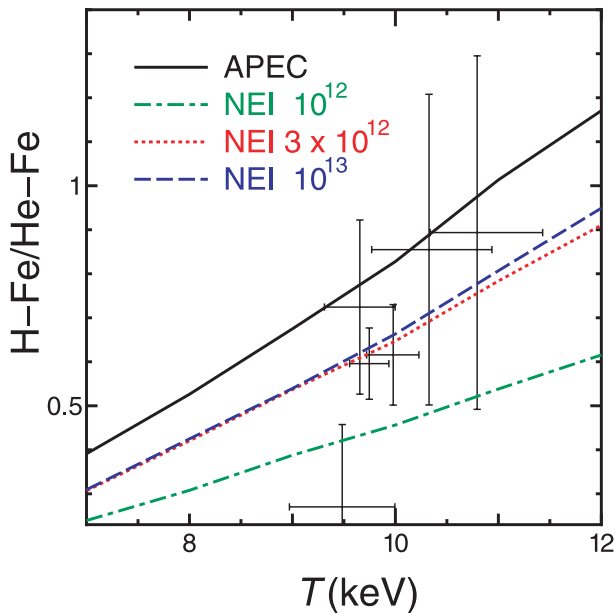


Fig. 9. Observed ratios of H-like and He-like Fe $K\alpha$ lines (crosses). The prediction of the APEC model is shown with the solid line, and those of the NEI model are shown with the dot-dashed line ($n_{e1} = 1 \times 10^{12} \text{ s cm}^{-3}$), the dotted line ($n_{e1} = 3 \times 10^{12} \text{ s cm}^{-3}$) and the dashed line ($n_{e1} = 1 \times 10^{13} \text{ s cm}^{-3}$)

could affect the results. However, we found that this is not likely to be the case. We observed the region around H 1705–250 with Suzaku with an exposure time of 15 ks. We then used the spectrum of this region as the background for a spectral fit of region W. In this case, the temperature is $kT = 9.7^{+0.9}_{-1.0}$ keV,

which is consistent with that in table 1. Another possibility is that the high temperature in these faint outer regions is due to stray light from the bright central regions of the cluster. For the X-ray telescopes carried on ASCA, such a problem was much more serious for ASCA than for Suzaku (Serlemitsos et al. 2007). Although Watanabe et al. (2001) took account of the effect in their analysis, the correction might not have been sufficient.

Although we could not find the cause of the inconsistency, we believe that the results of Suzaku are more reliable, because the problem of the stray light has been much improved.

8.2. The Cool Core

The existence of a cool core (section 4) and the isothermality of the cluster (section 3) indicate that the Ophiuchus cluster is a cool core cluster. While many clusters with medium temperatures (~ 5 keV) are cool core clusters having short central cooling times, most of the hottest clusters with temperatures similar to the Ophiuchus ($\gtrsim 10$ keV) do not seem to have cool cores (e.g., figures 18c,d in Ota & Mitsuda 2004). This is probably because the latter are major-merger clusters in which the core has been destroyed and the temperature has been boosted by the merger (Randall et al. 2002). For example, the extended HIFLUGCS sample includes 106 nearby clusters (Reiprich & Böhringer 2002). Among them, there are only 8 clusters, including the Ophiuchus cluster, with temperatures larger than 9.0 keV (Chen et al. 2007). Five of them (A 1689, A 1914, A 2163, A 2319, and Triangulum Australis) do not have a prominent cool core (Andersson & Madejski 2004; Govoni et al. 2004; White 2000). Although A 754 and A 2142 have a cool core, they are now undergoing a major merger (Markevitch et al. 2000; Govoni et al. 2004). Thus, the

Ophiuchus cluster seems to be exceptional in having a very high temperature and a cool core with no strong evidence of a major merger. Since clusters with cool cores tend to be old (e.g., Fujita & Takahara 2000; Ota et al. 2006), the Ophiuchus cluster would be exceptionally old, given its large mass. Contrary to merging clusters in which star-formation activities might be induced in the disk galaxies (e.g., Fujita & Nagashima 1999; Fujita et al. 1999), the environment in the Ophiuchus cluster might have been calm for a long time. Thus, it would be interesting to study the nature of the galaxies inside it.

8.3. Non-Thermal Hard X-Ray Emission

Most of the clusters from which non-thermal X-ray emission has been detected are major-merger clusters (Nevalainen et al. 2004). Since non-thermal synchrotron radio emission has often been observed from these clusters (Govoni & Feretti 2004), the non-thermal hard X-ray emission could be attributed to inverse Compton scattering of photons by the relativistic electrons that are responsible for the radio emission. Since the cooling time of these electrons ($\sim 10^8$ yr) is much shorter than the dynamical time-scale of a cluster ($\sim 10^9$ yr; Sarazin 1999), the electrons are likely to be primary electrons, which are now being directly accelerated at shocks or turbulence in the ICM induced by recent cluster mergers.

The hard X-ray excess detected by Eckert et al. (2008) from the Ophiuchus cluster is curious in this regard. Although a cluster merger does not always destroy a cool core (e.g., A 2142: Markevitch et al. 2001) and our temperature map (figure 3a) is coarse, the X-ray image and spectra from this cluster do not show any strong evidence for a major merger. One possibility is that the Ophiuchus cluster is currently undergoing an early stage, small impact parameter (head-on) merger with the merger axis being close to our line of sight. Then, the two merging subclusters would be projected on top of one another, and no azimuthal temperature variations would necessarily be expected. By the same argument, one would not necessarily expect any azimuthal variations in the mean redshift. Although the likelihood of a head-on collision along the line of sight is small, this hypothesis would appear to be consistent with the apparent regularity of Ophiuchus, the presence of a cool core (albeit without any very cool gas), and the presence of nonthermal hard X-ray emission due to a merger shock or turbulence.

On the other hand, if Ophiuchus is not really a merging cluster, then the nonthermal hard X-rays cannot be attributed to primary electrons accelerated through a recent major cluster merger, although we cannot rule out particle-acceleration by turbulence in the core generated by a minor merger (Fujita et al. 2004a, 2005; Mazzotta & Giacintucci 2008). One possibility is that particles might have been accelerated by the central AGN rather than a cluster merger, because the hard X-ray emission is observed at the center of the Ophiuchus cluster (Eckert et al. 2008). Moreover, since recent strong AGN activities have not been observed at the cluster center (Dunn & Fabian 2006), the non-thermal emission from the cluster may come from secondary electrons that are generated through proton-proton interaction (Pfrommer & Enßlin 2004). In this case, the non-thermal emission can be observed even long after

the AGN activities and proton acceleration cease, because the cooling time of the protons is longer than the age of a cluster. Recently, Fujita et al. (2007) proposed that the protons are accelerated at the forward shock around a cocoon created by an AGN outburst.

Another possible source of the non-thermal X-ray emission would be dark-matter annihilation (Profumo 2008, see also Totani 2004). In any case, a confirmation of the non-thermal emission in Ophiuchus with other instruments would also be very useful. The Swift/BAT instrument observed Ophiuchus for 1.3 Ms, and failed to detect any non-thermal hard X-ray emission (Ajello et al. 2008; Okajima et al. 2008). Based on a joint Chandra and Swift/BAT analysis (with Chandra used to constrain the thermal emission from the cluster), Ajello et al. (2008) found an upper limit of $4.5 \times 10^{-12} \text{ erg s}^{-1} \text{ cm}^{-2}$ (20–60 keV), which is inconsistent with the INTEGRAL detection at more than 2σ . We note that Eckert et al. (2008) fit the thermal emission from the cluster with a single temperature model with a temperature of 8.5 keV. We find that most of the cluster is hotter than this, in agreement with the results from Ajello et al. (2008) and Okajima et al. (2008). The difference with Eckert et al. (2008) may be due to the cool core in Ophiuchus. It is possible that a more complex thermal model may be needed for Ophiuchus, and might bring the INTEGRAL and Swift/BAT results into better agreement. Given the present disagreement of the INTEGRAL and Swift/BAT spectral results, the lack of evidence for a merger, and the lack of a modern radio detection of a halo or relic, we view the non-thermal detection in Ophiuchus as being tentative.

9. Summary

We observed the Ophiuchus cluster with Suzaku X-ray satellite. We found that the ICM of the cluster is hot ($kT \sim 9\text{--}10$ keV) and is almost isothermal, except for the core. Contrary to a previous study, we did not find extremely hot regions ($kT \sim 20$ keV) in the cluster. In the core, the temperature is smaller and the metal abundance is larger than those in the surrounding region. The radial velocity difference between different regions of the ICM is less than $\sim 3000 \text{ km s}^{-1}$. The iron line ratios in X-ray spectra suggest that the ICM has reached a ionization equilibrium. These features indicate that the Ophiuchus cluster is not a major-merger cluster, but is a so-called cool core cluster. This cluster would be an exceptional cluster, because most of the clusters with these temperatures ($\gtrsim 10$ keV) are major-merger clusters. Another possibility is that Ophiuchus is a nearly head-on merger with the merger axis nearly along our line of sight; such a model would be consistent with the observed properties of the cluster. We obtained the upper limit of hard X-ray excess, which is consistent with the recent detection with INTEGRAL and upper limit with Swift/BAT. Assuming that the Ophiuchus cluster is not a major-merger cluster, the origin of any hard X-ray excess may not be a recent major cluster merger.

The authors wish to thank A. Furuzawa, R. K. Smith, and N. Ota for useful comments. We also thank the Suzaku operations team for their support in planning and

executing these observations. Y. F., K. H., and M. T. were supported in part by a Grant-in-Aid from the Ministry of Education, Culture, Sports, Science and Technology of Japan (Y. F.: 17740162; K. H.: 16002004; M. T.: 16740105,

19740096). T. H. R. acknowledges support by the Deutsche Forschungsgemeinschaft through Emmy Noether Research Grant RE 1462. C. L. S. was supported by NASA Suzaku grants NNX06AI37G and NNX06AI44G.

References

- Ajello, M., et al. 2008, *ApJ*, in press (arXiv: 0809.0006)
- Andersson, K. E., & Madejski, G. M. 2004, *ApJ*, 607, 190
- Arnaud, K. A., Johnstone, R. M., Fabian, A. C., Crawford, C. S., Nulsen, P. E. J., Shafer, R. A., & Mushotzky, R. F. 1987, *MNRAS*, 227, 241
- Ascasibar, Y., & Markevitch, M. 2006, *ApJ*, 650, 102
- Blanton, E. L., Sarazin, C. L., & McNamara, B. R. 2003, *ApJ*, 585, 227
- Brunetti, G., & Blasi, P. 2005, *MNRAS*, 363, 1173
- Brunetti, G., Setti, G., Feretti, L., & Giovannini, G. 2001, *MNRAS*, 320, 365
- Cassano, R., & Brunetti, G. 2005, *MNRAS*, 357, 1313
- Chen, Y., Reiprich, T. H., Böhringer, H., Ikebe, Y., & Zhang, Y.-Y. 2007, *A&A*, 466, 805
- De Grandi, S., & Molendi, S. 2001, *ApJ*, 551, 153
- Dunn, R. J. H., & Fabian, A. C. 2006, *MNRAS*, 373, 959
- Dupke, R. A., & Bregman, J. N. 2006, *ApJ*, 639, 781
- Eckert, D., Produit, N., Paltani, S., Neronov, A., & Courvoisier, T. J.-L. 2008, *A&A*, 479, 27
- Finoguenov, A., Arnaud, M., & David, L. P. 2001, *ApJ*, 555, 191
- Fujita, Y., Kohri, K., Yamazaki, R., & Kino, M. 2007, *ApJ*, 663, L61
- Fujita, Y., Matsumoto, T., & Wada, K. 2004a, *ApJ*, 612, L9
- Fujita, Y., Matsumoto, T., Wada, K., & Furusho, T. 2005, *ApJ*, 619, L139
- Fujita, Y., & Nagashima, M. 1999, *ApJ*, 516, 619
- Fujita, Y., & Sarazin, C. L. 2001, *ApJ*, 563, 660
- Fujita, Y., Sarazin, C. L., Kempner, J. C., Rudnick, L., Slee, O. B., Roy, A. L., Andernach, H., & Ehle, M. 2002, *ApJ*, 575, 764
- Fujita, Y., Sarazin, C. L., Reiprich, T. H., Andernach, H., Ehle, M., Murgia, M., Rudnick, L., & Slee, O. B. 2004b, *ApJ*, 616, 157
- Fujita, Y., & Takahara, F. 2000, *PASJ*, 52, 317
- Fujita, Y., Takizawa, M., Nagashima, M., & Enoki, M. 1999, *PASJ*, 51, L1
- Fujita, Y., Takizawa, M., & Sarazin, C. L. 2003, *ApJ*, 584, 190
- Fujita, Y., Tawa, N., Hayashida, K., Takizawa, M., Matsumoto, H., Okabe, N., & Reiprich, T. H. 2008, *PASJ*, 60, S343
- Fukazawa, Y., Ohashi, T., Fabian, A. C., Canizares, C. R., Ikebe, Y., Makishima, K., Mushotzky, R. F., & Yamashita, K. 1994, *PASJ*, 46, L55
- Fusco-Femiano, R., Orlandini, M., Brunetti, G., Feretti, L., Giovannini, G., Grandi, P., & Setti, G. 2004, *ApJ*, 602, L73
- Govoni, F., & Feretti, L. 2004, *Int. J. Mod. Phys. D.*, 13, 1549
- Govoni, F., Markevitch, M., Vikhlinin, A., VanSpeybroeck, L., Feretti, L., & Giovannini, G. 2004, *ApJ*, 605, 695
- Inoue, S., Aharonian, F. A., & Sugiyama, N. 2005, *ApJ*, 628, L9
- Ishisaki, Y., et al. 2007, *PASJ*, 59, S113
- Jaffe, W. J. 1977, *ApJ*, 212, 1
- Johnston, M. D., Bradt, H. V., Doxsey, R. E., Margon, B., Marshall, F. E., & Schwartz, D. A. 1981, *ApJ*, 245, 799
- Kafuku, S., Yamauchi, M., Hattori, M., Kawai, N., & Matsuoka, M. 1992, *Frontiers Science Series*, 483
- Kang, H., Ryu, D., Cen, R., & Ostriker, J. P. 2007, *ApJ*, 669, 729
- Kawano, N., et al. 2008, *PASJ*, in press (arXiv: 0805.3582)
- Koyama, K., et al. 2007, *PASJ*, 59, S23
- Kushino, A., Ishisaki, Y., Morita, U., Yamasaki, N. Y., Ishida, M., Ohashi, T., & Ueda, Y. 2002, *PASJ*, 54, 327
- Lahav, O., Edge, A. C., Fabian, A. C., & Putney, A. 1989, *MNRAS*, 238, 881
- Markevitch, M., et al. 2000, *ApJ*, 541, 542
- Markevitch, M., Gonzalez, A. H., David, L., Vikhlinin, A., Murray, S., Forman, W., Jones, C., & Tucker, W. 2002, *ApJ*, 567, L27
- Markevitch, M., Vikhlinin, A., & Mazzotta, P. 2001, *ApJ*, 562, L153
- Mazzotta, P., & Giacintucci, S. 2008, *ApJ*, 675, L9
- Miniati, F., Ryu, D., Kang, H., & Jones, T. W. 2001, *ApJ*, 559, 59
- Mitsuda, K., et al. 2007, *PASJ*, 59, S1
- Nevalainen, J., Oosterbroek, T., Bonamente, M., Colafrancesco, S. 2004, *ApJ*, 608, 166
- Ohno, H., Takizawa, M., & Shibata, S. 2002, *ApJ*, 577, 658
- Okajima, T. et al. 2008, *ApJ*, submitted
- Okumura, Y., Tsunemi, H., Yamashita, K., Matsuoka, M., Koyama, K., Hayakawa, S., Masai, K., & Hughes, J. P. 1988, *PASJ*, 40, 639
- Ota, N., et al. 2007, *PASJ*, 59, S351
- Ota, N., et al. 2008, *A&A*, submitted (arXiv: 0805.0500)
- Ota, N., Kitayama, T., Masai, K., & Mitsuda, K. 2006, *ApJ*, 640, 673
- Ota, N., & Mitsuda, K. 2004, *A&A*, 428, 757
- Pfrommer, C., & Enßlin, T. A. 2004, *A&A*, 413, 17
- Piffaretti, R., Jetzer, Ph., Kaastra, J. S., & Tamura, T. 2005, *A&A*, 433, 101
- Pointecouteau, E., Arnaud, M., & Pratt, G. W. 2005, *A&A*, 435, 1
- Profumo, S. 2008, *Phys. Rev. D*, 77, 103510
- Randall, S. W., Sarazin, C. L., & Ricker, P. M. 2002, *ApJ*, 577, 579
- Reiprich, T. H., & Böhringer, H. 2002, *ApJ*, 567, 716
- Ricker, P. M., & Sarazin, C. L. 2001, *ApJ*, 561, 621
- Roland, J. 1981, *A&A*, 93, 407
- Rossetti, M., & Molendi, S. 2004, *A&A*, 414, L41
- Ryu, D., Kang, H., Hallman, E., & Jones, T. W. 2003, *ApJ*, 593, 599
- Sarazin, C. L. 1999, *ApJ*, 520, 529
- Schlickeiser, R., Sievers, A., & Thiemann, H. 1987, *A&A*, 182, 21
- Serlemitsos, P. J., et al. 2007, *PASJ*, 59, S9
- Smith, R. K., Brickhouse, N. S., Liedahl, D. A., & Raymond, J. C. 2001, *ApJ*, 556, L91
- Snowden, S. L., Egger, R., Finkbeiner, D. P., Freyberg, M. J., & Plucinsky, P. P. 1998, *ApJ*, 493, 715
- Takahashi, T., et al. 2007, *PASJ*, 59, S35
- Takizawa, M., & Naito, T. 2000, *ApJ*, 535, 586
- Tawa, N., et al. 2008, *PASJ*, 60, S11
- Totani, T. 2004, *Phys. Rev. Lett.*, 92, 191301
- Vikhlinin, A., Markevitch, M., Murray, S. S., Jones, C., Forman, W., & Van Speybroeck, L. 2005, *ApJ*, 628, 655
- Watanabe, M., Yamashita, K., Furuzawa, A., Kunieda, H., & Tawara, Y. 2001, *PASJ*, 53, 605
- White, D. A. 2000, *MNRAS*, 312, 663